Earth Planet. Sci. Lett. 625 (2024) 118488

Contents lists available at ScienceDirect

Earth and Planetary Science Letters

journal homepage: www.elsevier.com/locate/epsl

Shallow sources of upper mantle seismic anisotropy in East Africa

C.J. Ebinger [a,*], Miriam C. Reiss [b,1], Ian Bastow [c], Mary M. Karanja [d]

[a] Department of Earth and Environmental Sciences, Tulane University, New Orleans, LA, USA
[b] Institute of Geosciences, Goethe University Frankfurt, Frankfurt am Main 60438, Germany
[c] Imperial College London, London, UK
[d] Department of Geology, University of Nairobi, Nairobi, Kenya

ARTICLE INFO

Editor: Dr H Thybo

Keywords:
Shear-wave splitting
East African rift
Mantle flow
Oriented melt pockets

ABSTRACT

The East African rift overlies one or more mantle upwellings and it traverses heterogeneous Archaean-Paleozoic lithosphere rifted in Mesozoic and Cenozoic time. We re-analyze XKS shear wave splitting at publicly available stations to evaluate models for rifting above mantle plumes. We use consistent criteria to compare and contrast both splitting direction and strength, infilling critical gaps with new data from the Turkana Depression and North Tanzania Divergence sectors of the East African rift system. Our results show large spatial variations in the amount of splitting (0.1–2.5 s), with fast axes predominantly sub-parallel to the orientation of Cenozoic rifts underlain by thinned lithosphere with and without surface magmatism. The amount of splitting increases with lithospheric thinning and magmatic modification. Nowhere are fast axes perpendicular to the rift, arguing against the development of extensional strain fabrics. Thick cratons are characterized by small amounts of splitting ($\leq$0.5 s) with a variety of orientations that may characterize mantle plume flow. Splitting rotates to rift parallel and increases in strength over short distances into rift zones, implying a shallow depth range for the anisotropy in some places. The shallow source and correlation between splitting direction and the shape of upper mantle thin zones suggests that the combination of channel flow and oriented melt pockets contribute $>$ 1 s to the observed splitting delays. Enhanced flow, metasomatism, and melt intrusion at the lithosphere-asthenosphere boundary suggest that fluid infiltration to the base of the lithosphere may facilitate rifting of cratonic lithosphere.

1. Introduction

Lateral heterogeneities in crust and mantle structure influence the distribution of strain and magmatism in continental rift zones, yet the influence of plume-lithosphere interactions on melt generation and lithospheric strain patterns remain weakly constrained (e.g., Currie and van Wijk, 2016; Liu et al., 2021). The initiation of rifting in thick, cold continental lithosphere remains an outstanding problem in plate tectonics: the strength of lithosphere thicker than 100 km is more than the combined forces of gravitational potential energy and magma buoyancy forces, and is comparable to slab pull forces (e.g., Bialas et al., 2010; Stamps et al., 2010). Yet, active faulting with and without magmatism occurs in 150–200 km-thick Archaean lithosphere of the African plate in the absence of slab pull forces (e.g., Tiberi et al., 2019; Fishwick and Bastow, 2011), and rifting has occurred in other cratonic regions, such as the Proterozoic Mid-Continent rift (e.g., Bollmann et al., 2019). Rifting has also occurred in regions where the mantle lithosphere was previously heated and experienced melt extraction, creating both topographic relief at the lithosphere-asthenosphere boundary and compositional heterogeneities, as in parts of the Turkana Depression, Africa.

Mantle flow and applied forces contributing to rifting processes cause dislocation creep of mantle rocks, leading to crystallographic and lattice-preferred orientations (LPO) of minerals that produce seismic anisotropy of the bulk mantle aggregate (e.g., Nicolas and Christensen, 1987). A radially polarized shear-wave traversing an anisotropic material will split into orthogonal waves, with one polarization traveling faster than the other. Measurements of shear-wave splitting of core-refracted waves (e.g., SKS, SKKS, PKS, hereafter called XKS) yield the shear wave splitting parameters ϕ, the direction of the polarization plane of the fast shear wave, and δt, the delay-time between the fast and slow shear waves. The polarization plane of the fast shear wave gives insight into the orientation of the anisotropic axes, whereas the delay time is affected by the strength of the anisotropy and the thickness of the

* Corresponding author.
E-mail address: cebinger@tulane.edu (C.J. Ebinger).
[1] Now at Institute of Geosciences, Johannes Gutenberg University Mainz, Mainz, Germany.

https://doi.org/10.1016/j.epsl.2023.118488
Received 19 June 2023; Received in revised form 1 November 2023; Accepted 2 November 2023
Available online 17 November 2023

anisotropic layer beneath the seismograph (e.g., Silver and Chan, 1991; Becker et al., 2006). Mantle upwellings are expected to manifest as measurable anisotropic fabrics (e.g., Sleep et al., 2002; Becker et al., 2006). Other factors may influence SKS splitting measurements in rifts; preferentially-oriented melt pockets (OMP) in the mantle lithosphere and crust may contribute to observed anisotropy (e.g., Mainprice, 1997; Kendall et al., 2005; Holtzman and Kendall, 2010). In addition to melt-filled lenses, CO_2-rich fluids from deep magma sources may fill cracks and enrich the mantle lithosphere in anisotropic pyroxenites (e.g., Snyder and Lockhart, 2009).

Spatial patterns in the direction and strength of seismic anisotropy in melt-rich and melt-poor, tectonically active rift zones that formed above a broad mantle upwelling offer insights into bottom-up processes contributing to the initiation of rifting in cratonic lithosphere, as well as the role of pre-existing lithospheric heterogeneities in rifting processes. The East African rift system (EARS) formed above one or more low velocity zones rising from the core-mantle boundary to the base of the plate (e.g., Chang et al., 2020; Boyce et al., 2023). Yet, large data gaps and differences in the approach and treatment of SKS-splitting analyses between studies hampered comparative studies of upper mantle shear wave splitting patterns beneath eastern and central Africa, and few studies considered variations in the amount of splitting in their analyses (Fig. 2).

Our new XKS-splitting studies of the EAR offer unprecedented insights into rifting processes. We analyze new and existing data from eastern Africa using both splitting intensity and transverse energy minimization methods to evaluate spatial patterns in both the splitting direction and the amount of splitting (Fig. 2). New analyses include data from 1) the Turkana depression region that spans an area of unusually thin and comparatively melt-poor mantle (Kounoudis et al., 2021), enabling evaluation of upwelling mantle flow contributions and 2) the North Tanzania Divergence at the Tanzania craton boundary, which samples the sharp contrast between the flanks of a cratonic keel and adjacent rift zones, localized volcanic zones in the Eastern rift, and the Ethiopian flood basalt province > 100 km from the rift zone (Tiberi et al., 2019)(Supplementary Material, Tables SM1, SM2). The consistent analyses allow us to compare the direction and amount of splitting across deeply-rooted Archaean cratons, Proterozoic orogenic belts, Mesozoic rifts, and Cenozoic rifts with and without rift magmatism, as well as the Eo-Oligocene Ethiopian flood basalt province largely unaffected by extension.

While the absolute motion vector of the African plate is NNE from hotspot reference models (Doubrovine et al., 2012) and NE from no-net rotation models (e.g., Argus et al., 2011), the < 5 mm y^{-1} African plate velocity over the past 8–10 My is probably too slow to generate basal drag fabrics in the asthenosphere (e.g., Debayle and Ricard, 2013). East Africa is therefore an ideal study locale to address: Are splitting patterns dominated by NE-oriented upper mantle flow from the African superplume (e.g., Adriampenomanana et al., 2021), or is splitting dominated by strain fabrics in Archaean to Late Proterozoic lithosphere (e.g., Walker et al., 2004; Albaric et al., 2014)? Does extended lithosphere effectively channel asthenospheric flow along the rift axis, and is flow deflected by topographic relief at the lithosphere-asthenosphere boundary (e.g., Sleep et al., 2002; Holtzman and Kendall, 2010)? Do rift-parallel, fluid-filled fractures contribute to splitting (e.g., Kendall et al., 2005; Bastow et al., 2010)?

2. Background

2.1. Geodynamic and tectonic setting

The large African plate comprises several > 150 km-thick Archaean cratons that amalgamated during orogenies between ~2.5 - 0.5 Ga (e.g., Fritz et al., 2013). Proterozoic orogenies imparted a NW-fabric in areas now transected by parts of the Western rift (e.g., Boniface and Appel, 2018; Fritz et al., 2013). The Pan-African orogeny (950–550 Ma) imparted a predominantly N-S metamorphic fabric along much of the Indian Ocean margin of Africa when continental and oceanic lithosphere was accreted (e.g., Fritz et al., 2013; Fig. 3). Since the Pan-African, eastern Africa has experienced episodes of rifting in the Permo-Triassic, Cretaceous, and an enigmatic event in Paleogene time (e.g., Fig. 3).

The East African rift initiated after flood magmatism in Ethiopia at ~45 Ma, and fault bounded basins initiated by 27–30 Ma in the Red Sea, Turkana Depression (e.g., Ebinger et al., 2017; Fig. 3). Rift zones with and without magmatism separate semi-rigid plates whose boundaries remain poorly determined owing to the slow separation velocities as well as paucity of Global Navigation Satellite System (GNSS) observations (e.g., Saria et al., 2014; Birhanu et al., 2016; Daly et al., 2020; Knappe et al., 2020). The Main Ethiopian Rift (MER) marks the divergent plate boundary between the slowly opening (≤ 6 mm y^{-1}) Nubia and Somalia plates; ongoing magma intrusion leads to strain accommodation across parts of the uplifted plateau outside the MER (Birhanu et al., 2016). The Eastern rift separates the Victoria microplate from the Somalia plate where opening velocity is ~3 mm y^{-1} (e.g., Saria et al., 2014; Knappe et al., 2020) (Figs. 1, 3). The lack of seismicity and absence of upper mantle velocity variations between the Eastern and Western rift argue against a tectonic connection across the Turkana depression (Kounoudis et al., 2021; Musila et al., 2023). Opening rates across the Western rift are poorly determined owing to the absence of GNSS sites on the western side of the rift, or complicated by volcano inflation signals (e.g., Geirsson et al., 2017; Stamps et al., 2018).

Normal fault systems bounding the Western and Eastern rifts and MER strike sub-N-S, and formed in Proterozoic orogenic belts surrounding the unusually thick, strong, Archaean cratons (Fig. 1), suggesting that the pre-existing lithospheric thickness variations guided initial rift and magma localization (e.g., Sleep et al., 2002; Muirhead et al., 2020). Although segments of border and intrabasinal faults may parallel pre-existing shear zones (e.g., Daly et al., 2020), many steep border faults cut shallow basement fabric and show a regular along-axis segmentation that scales with plate strength (e.g., Ebinger et al., 1999). Obliquely-trending faults linking initially disconnected border faults are in many cases transtensional and may reactivate basement shear zones, but these are local features (e.g., Muirhead and Kattenhorn 2018; Musila et al., 2023). Stress inversions of earthquake source mechanisms spanning 40 km to surface and sparse GNSS data indicate sub-E-W extension throughout the study area (e.g., Lavayssière et al., 2019; Craig et al., 2011; Stamps et al., 2018; Musila et al., 2023).

The uplifted African continent overlies one or more mantle upwellings rising from the core-mantle boundary to the base of variable thickness continental and oceanic lithosphere (e.g., Ritsema et al., 2011; Chang et al., 2020; Boyce et al., 2023). Using new data from the Turkana region, Boyce et al. (2023) image three separate low velocity zones: one rooted beneath the Atlantic margin of S. Africa, and a second below the Indian Ocean north of Madagascar. The thinnest mantle transition zone beneath East Africa is below the NW Turkana Depression and northern Uganda and is underlain by a lower mantle plume tail; a possible third upwelling (Boyce et al., 2023). The Ethiopia-Yemen flood basalts may have overlain this thin MTZ at 40–45 Ma when flood magmatism initiated. Two or three plumes sampling different source zones can explain temporal and spatial variations in geochemistry of eruptive lavas (e.g., Pik and Hilton 2006). In some parts of the plateau areas, 1 and 2 km-thick lavas and isostatic compensation for 1–10 km of now frozen magma added to the base of the crust contribute to uplift (e.g., Chambers et al., 2019; Ogden et al., 2023). The timing of plume impingement is linked to the onset of flood basalt magmatism between ~45 and 35 Ma in southwestern Ethiopia, and a coeval period of kimberlite emplacement along the margins of Archaean cratons (Fig. 1).

The Ethiopia-Yemen and East-Central African plateaux are separated by an ~300 km-wide topographic depression that is underlain by crust stretched during Mesozoic and Palaeogene rifting: the Turkana depression (Fig. 2). The two plateaux are actually one dynamically uplifted

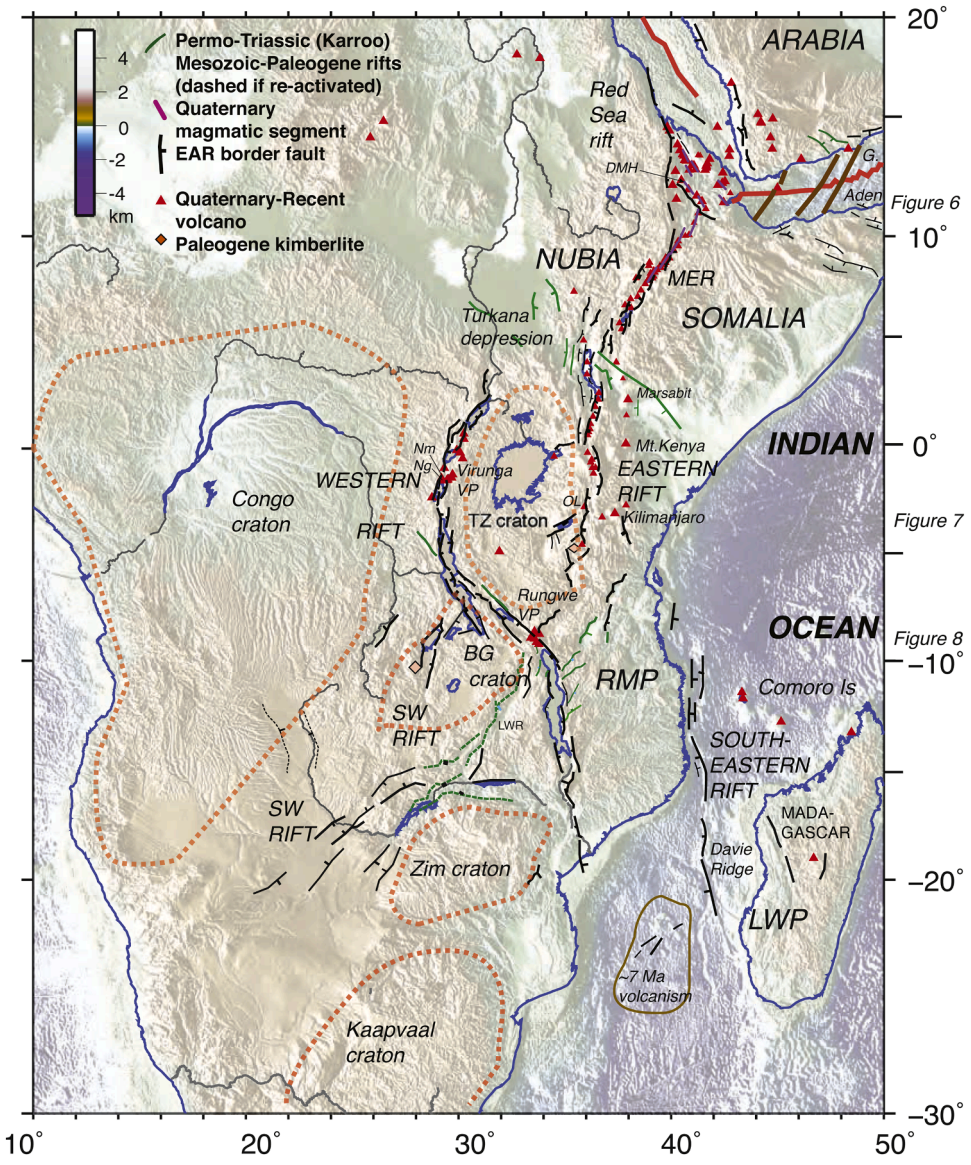

Fig. 1. Major fault systems of the Red Sea, Gulf of Aden, Main Ethiopian rift (MER), Eastern rift, Western rift, Southwestern (SW) rift, Southeastern rift and Comoros-Madagascar rift zones with respect to Nubia, Somalia, Arabia, and Rovuma (RMP), Victoria (TZ) and Lwandle (LWP) microplates, and the approximate boundaries of the Congo, Tanzania (TZ), Bangweulu (BG), Zimbabwe (Zim) and Kaapvaal Archaean cratons with $\geq$ 160 km-thick lithosphere. Green lines indicate Permian-Mesozoic normal faults associated with Gondwana breakup, and Paleogene faults that lie within the EAR (dashed if reactivated). The brown ellipse outlines an area of ~ 7 Ma magmatism and platform formation in the Indian Ocean between Africa and Madagascar. Nm is Nyamuragira volcano, Ng is Nyiragongo volcano. Pleistocene volcanoes from Global Volcanism Program (2013). Only faults that cut dated sedimentary sequences or dated lavas, or are seismically active are shown; it is likely that more fault systems are active. From Ebinger et al. (2017) updated with data from Daly et al. (2020) and Franke et al. (2015).

region extending from southern Africa to the Red Sea (Kounoudis et al., 2021; Ogden et al., 2023). The superposed episodes of rifting create a zone of pronounced crustal thinning that in large part explains the low elevation of the Turkana Depression (Ogden et al., 2023).

Between 35 and 15 Ma carbonatitic and alkali basaltic magmatism occurred in some areas now part of the Eastern and Western rift zones ringing the Tanzania craton (e.g., Roberts et al., 2012), suggesting that pre-existing lithospheric thickness variations may have influenced melt generation (e.g., Tiberi et al., 2019; Muirhead et al., 2020). Pleistocene-Recent magmatism occurs in a few isolated provinces in the Western rift, along the length of the Eastern rift and MER, at a kimberlite locale on the Tanzania craton, and across the Ethiopian plateau west of the MER (Figs. 1 and 3).

Most Miocene-Recent mantle xenoliths are metasomatized (e.g., Rudnick et al., 1998; Baptiste et al., 2015; Trestrail et al., 2017) (Fig. 2). The exception is peridotite xenoliths from Marsabit volcano that formed in lithosphere stretched during Cretaceous time; they lack metasomatic refertilization but show progressive thinning during cooling (Kaeser et al., 2006; Kaczmarek and Reddy, 2013) (Fig. 2). Peridotite and pyroxenite xenoliths from a nearby site (Mega) also show decompression from ~90 to 50 km (Tommasi et al., 2016; Casagli et al., 2017) (Fig. 2). Xenoliths from the southernmost Eastern rift and its flanks (Pello-Eledoi, Olmani, Chyulu Hills, Labait) sample much thicker and probably Archaean lithosphere affected by the percolation of carbonatitic fluids (e.g., Vauchez et al., 2005) (Fig. 2). Some xenoliths show deformation by dislocation creep at high deviatoric stresses beneath the current rift, and low deviatoric stress beneath the rift flanks (Baptiste et al., 2015). The Mega samples show $<$ 6% and $<$ 4% for P- and S-wave polarization anisotropy, respectively (Tommasi et al., 2016), compared to craton edge samples in the southern part of the Eastern rift that show 3.3–18.4% P-wave polarization anisotropy, and 2.3–13.2% S wave polarization anisotropy (Baptiste et al., 2015). Considered together, the

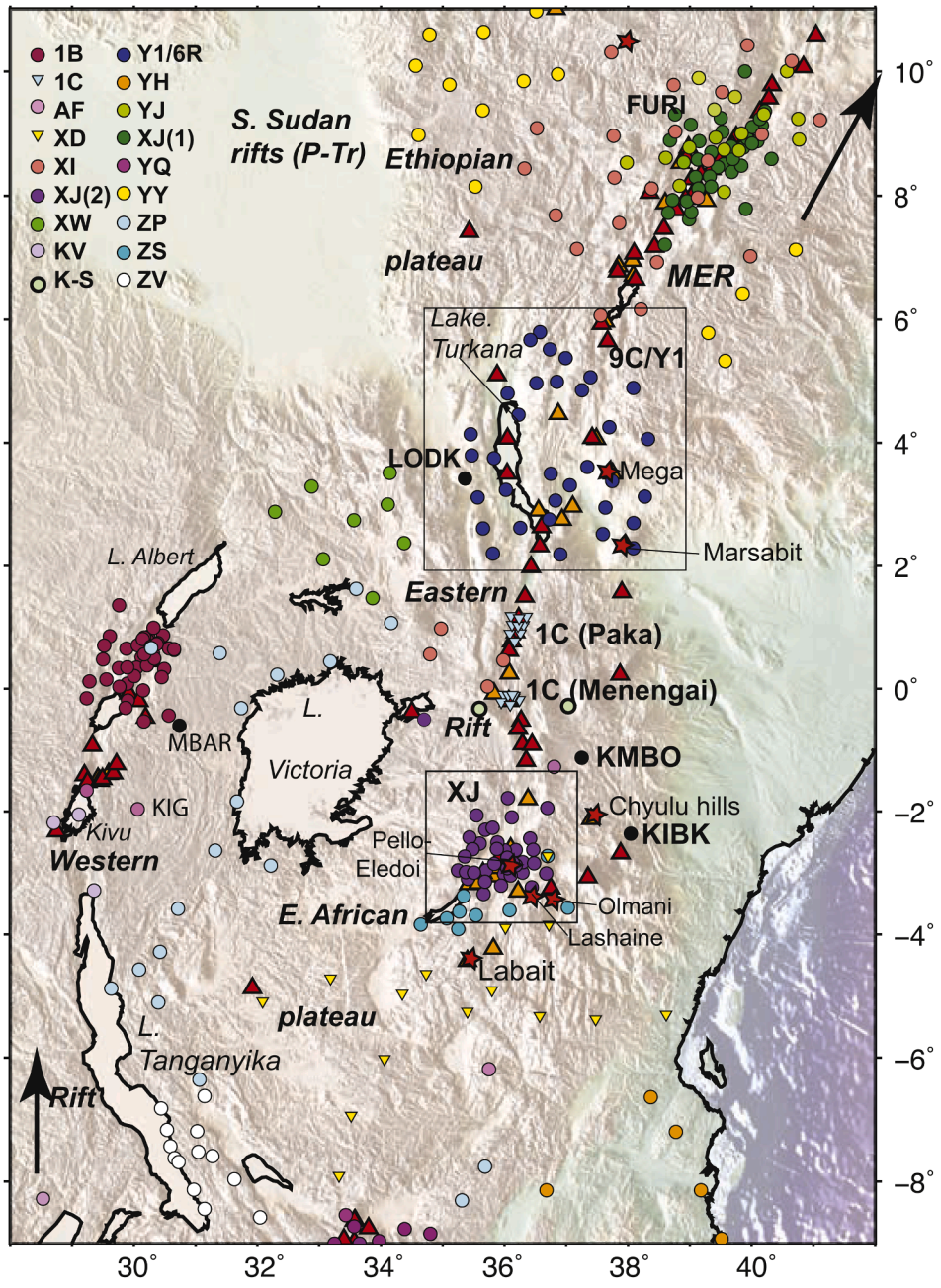

Fig. 2. Distribution of seismic networks analyzed in this study. Black circles are permanent stations of the Global Seismic Network and GEONET (see Table SM2 for data sources). K-S is Kenya-Sweden project. Boxes enclose CRAFTI (XJ2), TRAILS (Y1/6R); Paka and Menengai volcano arrays (1C). Red stars: mantle xenolith locales (Mega, Marsabit, Chyulu Hills, Pello-Eledoi, Labait, Lashaine, and Olmani). Orange triangles: Pleistocene volcanic centers; Red triangles: Holocene eruptive centers. Black arrows: absolute plate motion in not net rotation reference after Conrad and Behn (2010).

mantle xenolith data, as well as magma chemistry indicate that the lower lithosphere has been heated and thinned, and it has been refertilized with C—O-H-rich fluids, but in a spatially heterogeneous pattern. This metasomatism could remove any pre-existing strain fabrics, and introduce new fabrics in gabbroic rocks (e.g., Snyder and Lockhart 2009).

2.2. *Previous investigations of seismic anisotropy and mantle deformation in east Africa*

Previous shear wave splitting (Table SM2, Fig. SM2) and analyses of radial and azimuthal anisotropy of surface waves show several consistent patterns (e.g., Bastow et al., 2010; Kendall et al., 2005). In rift sectors with surface expressions of rift magmatism, the fast S-wave polarization, or splitting direction is parallel to rift bounding structures and the orientations of dikes, suggesting that oriented melt pockets (OMP) in the mantle lithosphere and crust contribute to the observed along-axis splitting patterns (e.g., Gao et al., 1997; Kendall et al., 2005). Enhanced mantle flow along lithospheric thin zones that are broader than the surface expression of the rift may also contribute to rift-parallel anisotropy (e.g., Holtzman and Kendall 2010; Bastow et al., 2010; Tepp et al., 2018). Adriampenomanana et al. (2021) interpret primarily NNE and N-S splitting directions throughout East Africa as LPO primarily created by NE-directed Africa Superplume flow distributed throughout the upper mantle. Walker et al. (2004) found considerable spatial variability in terms of ϕ and δt across the Tanzania craton, and they interpreted patterns as evidence for fossilized strain fabrics from cratonic collisions. Tommasi and Vauchez (2015) used numerical models to

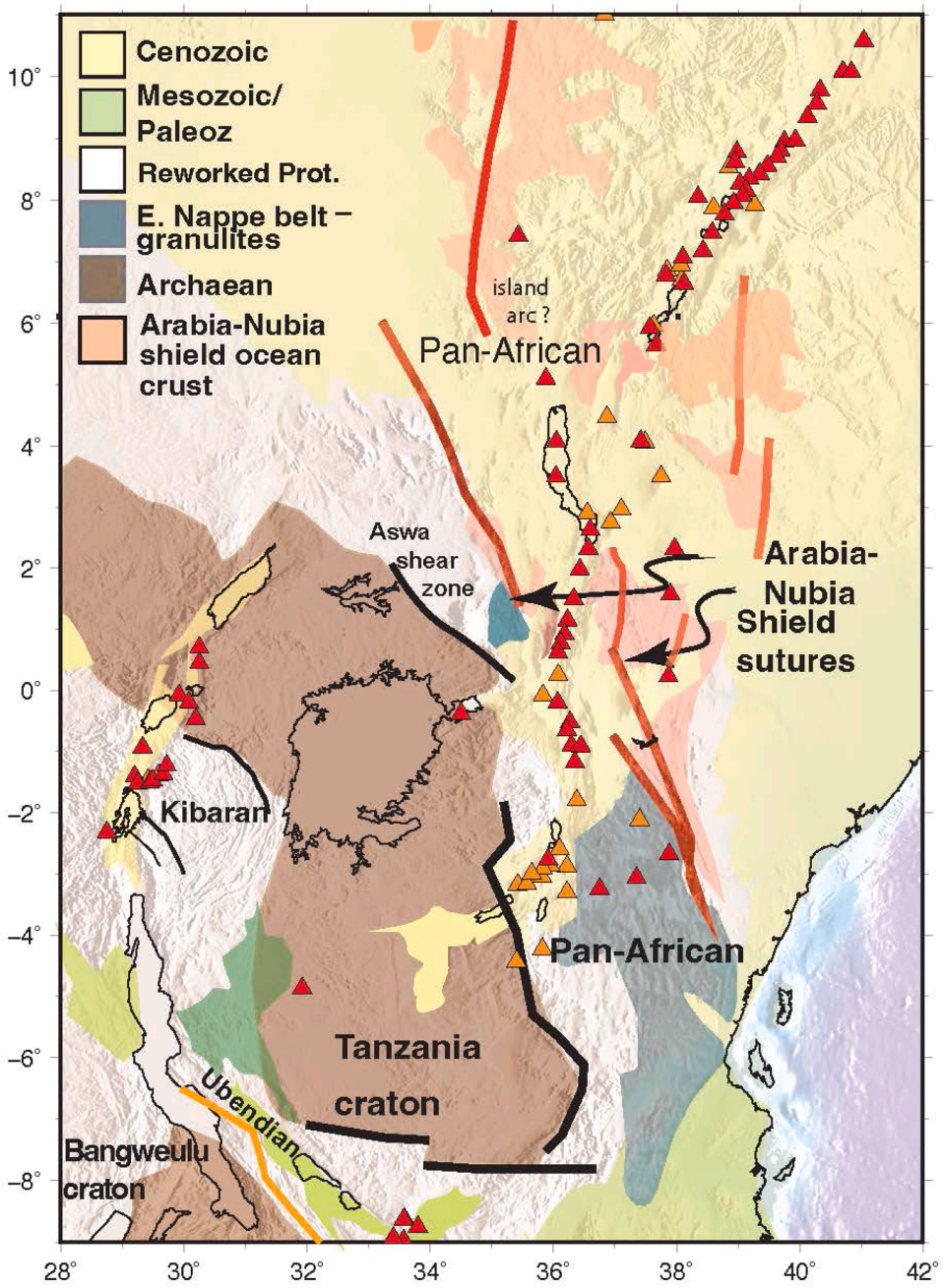

Fig. 3. Crustal tectonic domains after Fritz et al. (2013) and Boniface and Appel (2018). Archean cratons have unusually thick lithosphere (> 150 km), compared to 100–120 km-thick Proterozoic orogenic belts, and ≤ 100 km-thick Mesozoic passive margins (e.g., Fishwick and Bastow, 2011). Black lines-Proterozoic sutures; red lines-Pan-African sutures; orange line-Pan-African reactivation; orange triangles- Pleistocene volcanic centers; red triangles-Holocene eruptive centers.

demonstrate the effects of fossilized crystallographic preferred orientation of mantle materials on XKS measurements.

Reiss et al. (2019) considered lower mantle contributions to anisotropy from the large low shear velocity province (LLSVP) beneath Africa through comparison of SKS and SKKS phases, and found contributions to anisotropy along the steep margins of the LLSVP and within an ultra-low veolcity zone inside the LLSVP. The influence of the D" anisotropy is similar throughout the region we analyze except for the NE corner of our study area, where D" anisotropy is stronger (Reiss et al., 2019). Accordingly, XKS measurements in the selected area most likely sample upper mantle anisotropy.

3. Methods and data

3.1. Methods

P-to-S conversions at the core-mantle boundary provide an opportunity to measure upper mantle seismic anisotropy below a seismograph station (e.g., Silver and Chan 1991). At distance ranges of 88–130°, teleseismic body-waves arrive with near vertical incidence angles (< ~15°), making the distance traveled through the anisotropic layer close to the thickness of the layer.

We use SplitRacer 2.0 (Reiss and Rümpker, 2017), which uses observations in 50 randomly selected time windows, to facilitate all aspects of the data analyses. We use both the transverse component minimization (TCM) method of Silver and Chan (1991) and the multichannel

method of Chevrot (2000) as implemented in Reiss et al. (2019). After transforming waveforms to radial and transverse components, the TCM method utilizes a grid-search over all combinations of ϕ and δt to best minimize the transverse component energy (energy minimization), effectively removing the effect of splitting on individual waveforms. Here we also use SplitRacer's option to analyze all data at a given station in one grid search which then results in a single combination of ϕ and δt that best reduces the transverse energy of all waveforms simultaneously. The multichannel method measures the splitting intensity, which is derived from the amplitude ratio between the transverse component and the time derivative of the radial component, on individual XKS waveforms (Chevrot, 2000). Assuming a reasonable distribution of phases in backazimuth of the teleseisms recorded at each station, the observed splitting intensities map a sinusoid whose phase and amplitude define the fast direction and delay time (e.g., Fig. SM1, Table SM1).

3.2. Data

We process and analyze data from five temporary arrays (1C, Y1/6R, XJ, YY, Sweden-Kenya), three permanent stations in the Eastern rift (KIBK, LODK, KMBO), and four permanent stations in the Western rift and its flanks (MBAR, BUJA, IDJ, LWI) (Fig. 2, Table SM2). In addition to these new measurements, we re-analyze data from publicly available data from African networks (Table SM2; Fig. 2). Data from network 1B in Uganda was analyzed using the same approach; the results of Homuth et al. (2016) are used. With all other data sets, we considered teleseisms of moment magnitude 5.9 and greater at epicentral distances between 88° and 130° We identified high-quality XKS waveforms for analysis through both automated and visual checking for signal-to-noise ratio > 2, good waveform clarity, and measured initial polarizations within 10° of the backazimuth. For example, for station STCK, the energy is zero when the XKS wave is polarized parallel or perpendicular to the fast axis of the anisotropic material, and maximized when the polarization is 45° from the bulk symmetry axis of the aggregate material (Fig. 4). We filter using a zero phase Butterworth bandpass filter with corner frequencies of 0.02–0.25 s (see Supplementary Materials). Null measurements were determined by the initial linearity of the particle motion and the lack of signal on the transverse component (e.g., Reiss and Rümpker 2017).

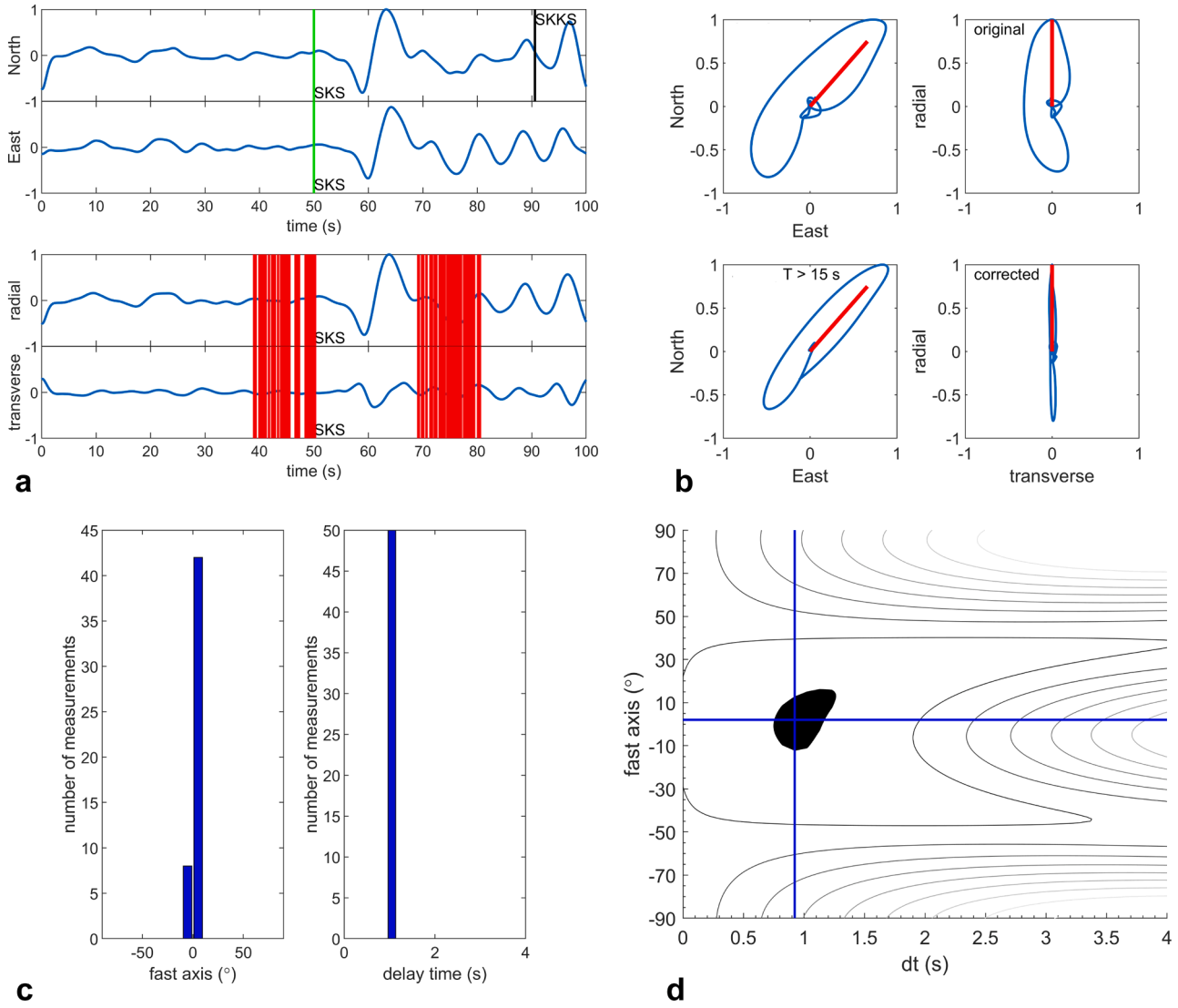

Fig. 4. Transverse component minimization analyses of an SKS phase recorded at station STCK from network Y1/6R. (a) Normalized radial and transverse components. The red bars denote 50 randomly selected time windows used for the analysis. (b) Particle motions for different periods and time windows. The top left panel corresponds to the entire time window of 100 s. Other panels show the particle motion for a selected time window surrounding the phase of interest (SKS). The red bar indicates the back azimuth. (c) Histogram of splitting parameters for the randomly selected time windows. (d) Energy grid of the corrected transverse component. The blackened contour level refers to the 95% confidence level. The blue cross marks the pair of splitting parameters which minimizes the energy on the transverse component.

Additional criteria were the initial ellipticity of the particle motion, the linearity of the corrected particle motion, the waveform quality, the similarity of the fast and slow split shear waveforms.

All splitting measurements present path-integrated results. Splitting intensity measurements alone cannot be used to infer multi-layered anisotropy whereas TCM can provide information on multiple layers if results from different backazimuths are available (e.g., Chevrot 2006; Silver and Long 2011). If e.g. two anisotropic layers are present, φ and δt display a typical 90°-periodicity with the backazimuth. However, splitting intensity measurements can result in meaningful measurements even where there is a weak signal in the transverse component close to null, whereas the TCM method may fail to detect small δt (e.g., Lopes et al., 2020). Used together, the TCM and splitting intensity measurements enable insights in areas with complex anisotropy, including variations with backazimuth resulting from multiple anisotropic layers and local variations in mantle structure.

3.3. Data selection

We illustrate our approach using the four networks (CRAFTI-CoLi-BREA, TRAILS, 1C, YY) analyzed for the first time. Thirty-four teleseismic earthquakes of $M_W \geq 5.9$ at distances between 88 and 130° recorded on the CRAFTI (XJ) temporary array between January 2013 and December 2014 provided results that satisfied our 'good' criteria: signal-to-noise ratios > 2, energy reduction > 50%, no interference with non-XKS phases (e.g., Fig. 5). Eighty-seven teleseisms of $M_W \geq 6.0$ at distances between 88° and 130° recorded on the TRAILS network (Y1 and 6R) between January 2019 and October 2021 in the Kenya, and two additional stations from the Sweden-Kenya partnership infill a large gap between the ER and MER (Fig. 3). For the permanent stations (LODK, KIBK, KMBO), 46 teleseisms of $M_W \geq 6.0$ at distances between 88°-130° were used (Figs. 2 and 5). Fifty-nine teleseismic earthquakes of $M_W \geq 6.0$ at distances between 88° and 130° recorded on network 1C in the Kenya rift near the geothermal prospects of Paka and Menengai volcanoes provided good results (Fig. 3). For both permanent and temporary arrays, azimuthal coverage is excellent (Fig. 5).

A critical part of our analyses is to place the new results within a regional context, and to interpret both splitting direction, φ, and amount of splitting, δt. Previous XKS-splitting studies in Africa have used different filters, or a single window rather than the 50 utilized in this study, and rarely has splitting intensity been considered. We chose to re-analyze published and accessible data to enable comparison of splitting direction, strength, as well as splitting intensity, which is more accurate in areas with small amounts of splitting (e.g., Lopes et al., 2020). We report results at stations where four or more non-null measurements are made, and report null where 5 or more null measurements are made.

The back-azimuths of null measurements are approximately perpendicular or parallel to measured ϕ (Fig SM2). Null measurements can occur from (1) alignment with the fast or slow splitting direction, (2) multiple anisotropic layers that cancel each other out (e.g., Barruol and Hoffmann, 1999), or 3) lack of azimuthal anisotropy. Our null measurements are consistent with the first interpretation on most stations, where non-nulls are also detected. The relatively short time period of observations at temporary seismic stations did not afford azimuthal coverage adequate to evaluate the presence or absence of two-layer splitting. At the permanent sites in the Eastern rift, we found little evidence for two-layer splitting: azimuthal variations in splitting direction and intensity are small and two-layer models showed similar splitting in both layers (Figure SM3).

4. Results

For all of the data sets, we first evaluated sensor orientations from analyses of teleseismic arrivals, with few sites showing deviations greater than ± 5°. Both TCM and splitting intensity measurements were made for each station, as reported in Tables SM1, SM2. Comparison of results using the two methods shows that the results are identical, within uncertainties, for both ϕ and δt for the new data. For individual measurements, the splitting intensity method typically provides a lower δt error but a slightly higher error in ϕ (e.g., Reiss et al., 2019). New and re-analyzed SKS-splitting patterns are presented in Fig. 6, with an enlargement of the new data from the Eastern rift shown in Figure SM3.

We equate 'rift zone' with the 200–300 km-wide swath of faulted basins as well as their flexurally uplifted rift flanks; this breadth captures the wider zone of mantle lithospheric thinning as compared to the breadth of the fault bounded rift valleys. The Eastern rift is sub-N-S trending and perpendicular to its approximately E-W opening direction (Saria et al., 2014; Birhanu et al., 2016; Knappe et al., 2020). In the Western rift zone, modern extension direction rotates from WNW in the north to sub-E-W south of Lake Kivu (e.g., Stamps et al., 2018). The modern extension direction in the ENE-trending MER is WNW-ESE to E-W (Birhanu et al., 2016).

Within the Western rift, Eastern rift, and MER, fast splitting directions are sub-parallel to the sub-N-S-striking rift boundary fault

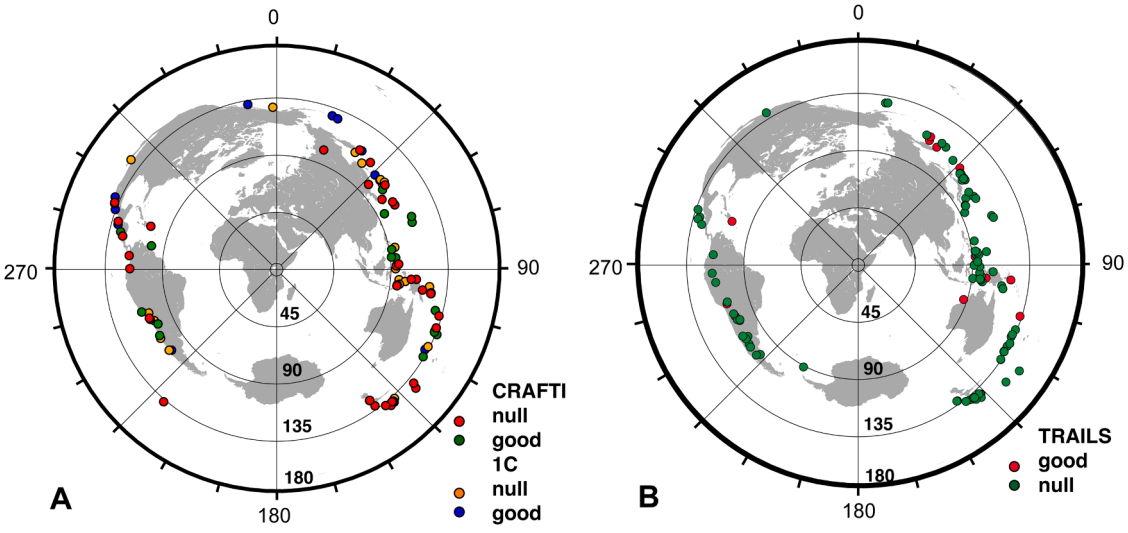

Fig. 5. (A) Azimuthal distribution of teleseisms used in analyses of CRAFTI (XJ) and Paka-Menengai (1C) experiments. Null measurements are determined from most azimuths for both temporary arrays. (B) Azimuthal distribution of teleseismic used in analyses of the TRAILS network in Kenya (Y1) and Ethiopia (6R), respectively (Tables SM1–2).

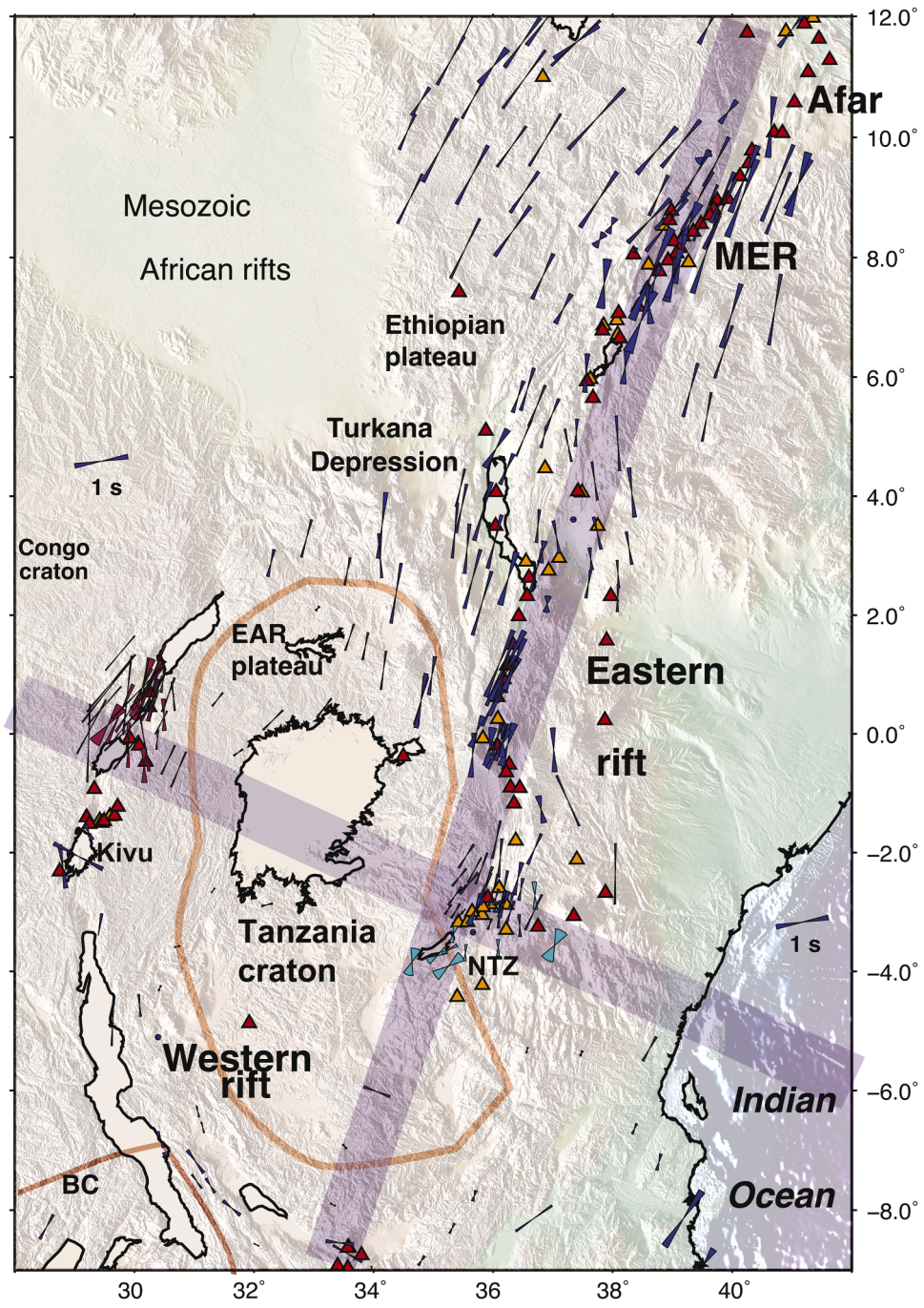

Fig. 6. New XKS splitting observations from energy minimization in dark blue; wedge width indicates 95% confidence limits. Re-analyzed data from Albaric et al. (2014) are shaded aqua to distinguish from the CRAFTI network. Burgundy wedge indicating 95% confidence limits from Homuth et al. (2016). Brown lines indicate the surface contact of Archaean and Proterozoic crust; northern margin is debated. Orange triangles are Pleistocene volcanoes; red triangles indicate Holocene volcanoes. NTZ is N. Tanzania Divergence; Kivu is sector with rift perpendicular measurement. Purple bands denote areas of data projected onto line of profiles shown in Fig. 7.

systems that, in some areas, parallel pre-existing shear zones and metamorphic fabric of Proterozoic orogenic belts (e.g., Kolawole et al., 2018), and reactivate the Mesozoic Rukwa fault (Roberts et al., 2012) (Figs. 1, 3 and 6). In turn, some of the border fault systems parallel the strike of basement lineations. Outside the rift zone within the Pan-African and other Proterozoic orogenic belts of the Western rift, splitting directions are generally NE, but with $\delta t < 1$ s. Exceptions are the southern part of our study area at stations within Permo-Triassic rift zones where δt is ~1 s. Some of these Permo-Triassic basins show evidence of re-activation in Pliocene-Recent time (e.g., Ebinger et al., 2017). A second exception is the Pan-African belt between the Tanzania craton and the Eastern rift. The lithosphere in this region was modified by magmatism at 30–18 Ma continuing to Holocene in some areas (Fig. 3).

Within the Tanzania and Bangweulu cratons the fast direction is spatially variable (NW, N-S, NE), and δt is small ($\leq$ 0.5 s). The orientations of fast axes rotate to directions sub-parallel to craton margins over distances < 100 km, and δt increases, as in the north Tanzanian Divergence (Fig. SM3). Splitting patterns within the Pan-African orogen unaffected by Cenozoic magmatism show a NE orientation with $\delta t \leq 1$ s

in the southeast along the northern edge of the Tanzania craton. This orientation parallels the NE-trending crustal fabric and ancient dikes imaged in aeromagnetic data and is oblique to N-S to NNE-striking rift faults (e.g., Albaric et al., 2014).

5. Discussion

The spatial detail afforded by the new, dense seismic networks as well as the consistent approach to quality control in the determination of best-fitting φ and δt enables us to compare their spatial variations 1) with lithospheric thickness variations at craton-orogenic belt boundaries and beneath the Cenozoic East African rift system, 2) zones with and without magma intrusion, and 3) lithospheric strain fabrics. Our splitting directions are generally consistent with the orientations of fast splitting directions from earlier studies (Figure SM2), but we report significant reductions in the amount of splitting in many areas. Another major difference is that our compilation is smaller than the catalog data base (e.g., Rajaonarison et al., 2023) owing to the omission of sites with fewer than 4 good/null measurements (compare Figs. 6, SM2 and SM3). All single splitting measurements are shown in Fig. SM2, even for sites with fewer than 4 good/null measurements.

5.1. Extension, faulting and magma intrusion

Throughout the study area, fast axes parallel the extensional basins and dikes that vary from NNW-striking in the southern part of the Western rift to NNE-striking along its northern sector, and N-S to NNE along the Eastern rift and MER (Figs. 1, 6). Data from dense arrays at the edges of the Tanzania craton provide additional insights into the mantle layer(s) contributing to the observed anisotropy patterns. The CRAFTI data from the eastern side of the Tanzania craton show a shift from NE to N-S splitting over a distance of 20–30 km (Fig. 6, SM2). Using the Fresnel zone models of Rümpker and Ryberg (2000), the minimum Fresnel zone width is 60–70 km depth for an assumed 80 km-thick lithosphere. Fresnel zones in the sub-lithospheric mantle overlap, requiring the anisotropy to reside within the lithosphere. A similar pattern was found along the NW margin of the Tanzania craton by Homuth et al. (2016). The magma-poor southern Tanganyika rift also shows a shift from NE-directed splitting outside the rift, to rift-parallel (NNW) over short length scales (Fig. 6). These changes in direction and amount of splitting over short spatial scales argue for anisotropy concentrated in the mantle lithosphere and uppermost asthenosphere.

We see little evidence for rift perpendicular strain fabrics (Figs. 3, 6), as reported by Eilon et al. (2014) in the back-arc system of Papua New Guinea. Instead, φ in the Eastern rift is roughly N-S, which is perpendicular to the N90°E extension direction (Saria et al., 2014; Knappe et al., 2020). In the MER and Ethiopian plateau the fast direction is NNE, again perpendicular to rift opening direction of ~N106 (Birhanu et al., 2016). Likewise, the NNW and NNE φ orientations in the southern and northern sectors of the Western rift are perpendicular to rift opening direction (e.g., Lavayssière et al., 2019; Homuth et al., 2016; Stamps et al., 2018). The exception is the ~1 s of WNW-directed splitting at a single station in the Kivu rift (Fig. 6) where the IDJ station is sited near the surface expression of a Proterozoic shear zone with the same strike (Figs. 3 and 6).

5.2. Ancient lithospheric strain fabrics

The rift parallel anisotropy observed in magma-poor and magma-rich sectors, regardless of age or fabric of lithosphere undergoing extension, argues against fossil strain fabrics as the primary contributor to observed XKS-splitting patterns within the modern extensional provinces (e.g., Walker et al., 2004). Outside the rifts and Ethiopian flood basalt province, splitting direction is predominantly NE, oblique to the ~N-S orientation of thrusts and sutures in the Pan-African. Some areas show little evidence for parallelism with ancient shear fabrics. For example, fast splitting direction shows no deviation from N-S to NNW near the lithospheric-scale Aswa shear zone (Figs. 3, 6, SM2). Mantle tomographic imaging in southwestern Ethiopia defines a NW-striking high velocity zone in the upper mantle associated with a NW-trending accreted Pan-African terrane (Kounoudis et al., 2021), yet fast directions are NNE and show little change regionally (Fig. 6). South and east of the Eastern rift splitting is oriented NE to E-W, whereas Pan-African recumbent folds and shear zones strike N-S (Figs. 6, SM2). The WNW-trending suture zones between the Tanzania and Bangweulu craton are oblique to the NNW and N-S φ directions we observed. Instead, fast directions parallel the shape of the lithospheric thin zones imaged tomographically and with receiver functions (e.g., Wölbern et al., 2012; Hopper et al., 2020). Weak anisotropy (< 1 s) may be caused by pre-existing strain fabrics in the lithosphere in all or some parts of the rift zones, as indicated by xenolith data; strain fabrics may contribute to the observed delay times.

5.3. Superplume dynamics

The direction of XKS-splitting we determine follows the general NE-directed upper mantle strain patterns predicted by the African Superplume spanning the upper mantle (e.g., Andriampenomanana et al., 2021; Rajaonarisan et al., 2023), with notable exceptions in the southern part of the Western rift where NNW splitting parallels the Bangweulu and Tanzania craton margins. The spatial variations in strength of splitting require additional processes: the smallest amounts of splitting occur outside the extensional provinces; the largest amounts of splitting are in areas with magmatism and lithospheric thinning. For example, δt increases from 1.5 s in the Turkana depression to more than 2 s across the broad Ethiopian plateau.

5.4. Rifting model

The amount of splitting is largest in the rift zones and flood basalt provinces, and smallest in the Archaean cratons, as shown in a WNW-ESE-trending profile spanning the Western rift, Tanzania craton, Eastern rift and Pan-African belt and a SSW-NNE-trending profile from the Malawi rift at the southern end of the Western rift, along the length of the Eastern rift to the MER (Fig. 7). For example, δt is less than 0.5 s in the Tanzania craton, less than 1 s in the north Tanzania Divergence area where magmatism and extension initiated after 7 Ma, and it increases to more than 1.5 s in the Turkana Depression where magmatism and extension initiated after ~30 Ma. The amount of splitting on the largely unfaulted Ethiopian flood basalt province is comparable to that in the MER where lithospheric thinning is 25% (e.g., Bastow et al., 2010); channeled flow alone cannot explain these patterns. The small amounts of anisotropy and large percentage of null measurements beneath cratonic regions may be related to their long and complex history, as well as the lack of metasomatism and magma intrusion during present day rifting. Summarizing, rift parallel anisotropy is observed in both magma-rich and magma-poor rift sectors, the primary anisotropic zone is in the upper asthenosphere and mantle lithosphere, and δt increases in areas with magmatism, with the largest amounts of splitting in the Ethiopian flood basalt province.

Multiple lines of reasoning lead us to deduce that contributions to anisotropy from LPO fabrics throughout the upper mantle are small, owing to the $\leq$ 1 s of NE-directed splitting observed outside the rift and magmatic zones (Fig. 7). Instead, the more than 1 s delay time, observed parallelism of splitting directions with zones of lithospheric thinning and magmatism, and indications for shallow sources of anisotropy argue for primary contributions from channeled along-axis flow and oriented melt pockets. Fossil strain fabrics in the mantle lithosphere may also contribute, but the weak anisotropy outside the rift suggests that these fabrics contribute < 1 s to the observed delay times.

Mantle xenoliths indicate up to 50% thinning of mantle lithosphere, and percolation of fluids with 2–13% S wave-anisotropy (Baptiste et al.,

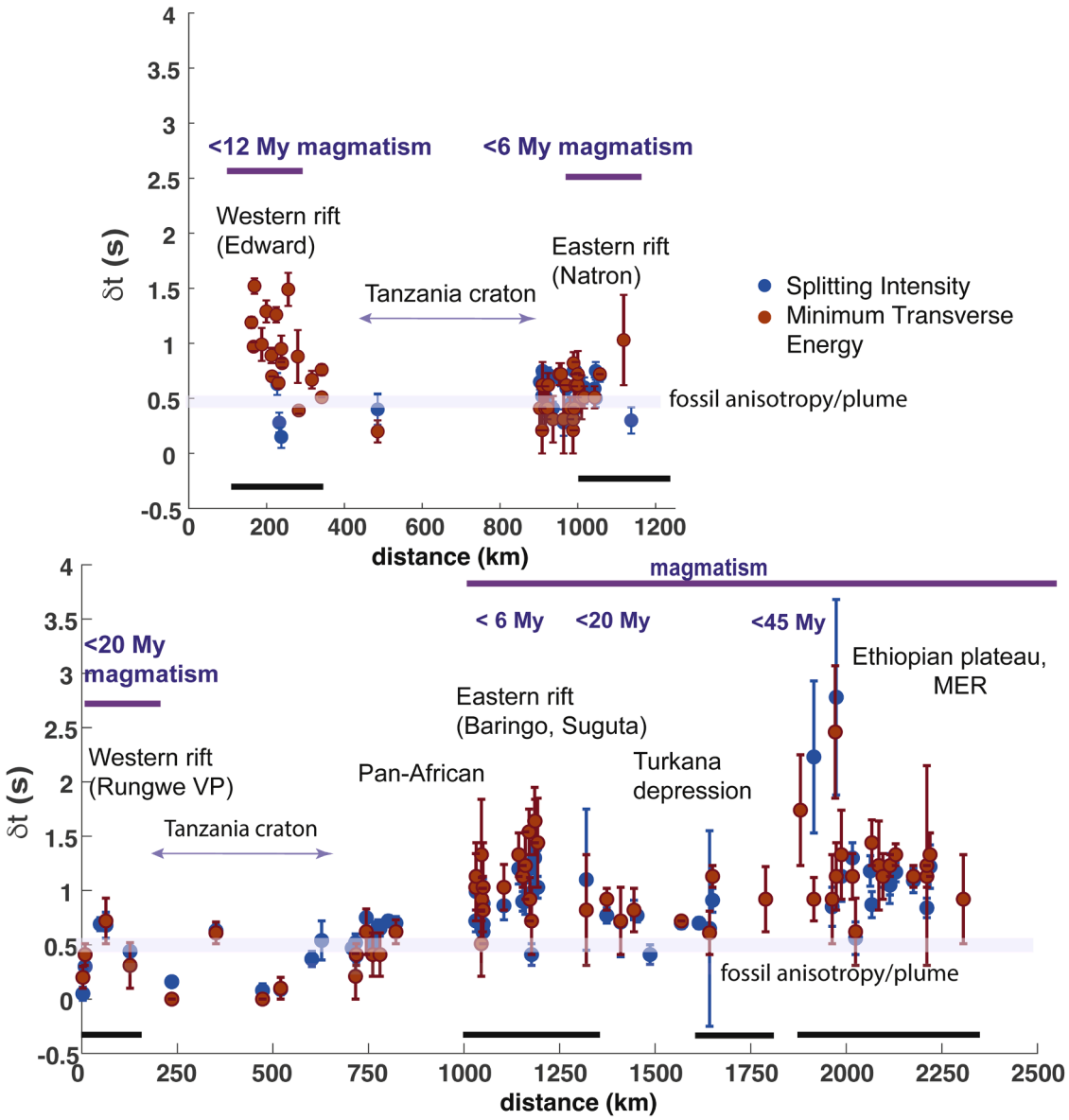

Fig. 7. Comparison of amount of splitting (δ_t) along (a) a WNW-ESE transect of the East African rift crossing the Archaean Tanzania craton and (b) a SSW to NNE transect from the Rungwe volcanic province at the northern end of the Malawi rift along the Eastern rift and Main Ethiopian rift, crossing parts of the uplifted Ethiopian plateau and Eo-Oligocene flood basalt province (Fig. 6). Data from ±50 km from the line were projected onto the line of the profile. Bold black lines indicate zones of lithospheric thinning. Gray line indicates average δ_t value outside rift zones, which we interpret as the combined contributions of fossil crust and mantle strain fabrics, as well as mantle plume flow contribution. The smallest amounts of splitting are found beneath the > 150 km-thick Tanzania craton, whereas the largest amounts of splitting (≥ 1.5 s) are observed across the Ethiopian flood basalt province, parts of which have experienced rifting over the past ~20 My. The Turkana depression is a region of lithospheric thinning during Mesozoic time, as well as the past ~27 My of extension and rift-related magmatism (e.g., Ogden et al., 2023).

2015). Seismic imaging in some parts of the rift indicate 50 km or more relief at the LAB beneath rift zones (e.g., Tiberi et al., 2019; Hopper et al., 2020). The 1–1.5 s of splitting in the weakly magmatic Turkana rift (Eastern rift) and the Albertine-Rwenzori zone (Western rift) may be representative of the combined along-axis flow contribution and fossil strain fabrics.

Melt preferentially ponds in zones of thinner lithosphere, spatially linking the channeled flow and melt and injection zones (e.g., Sleep et al., 2002) (Fig. 8). Aligned melt bodies and fluid-filled cracks in the lithosphere can produce rift-parallel splitting strength of ~1 s (e.g., Holtzman and Kendall 2010; Hammond and Kendall 2016). Where magma intrusion is localized, crustal contributions to splitting may be ~0.3–0.5 s (e.g., Kendall et al., 2005). Sharp contrasts in lithospheric thickness variations at the lithosphere-asthenosphere boundary may cause deflections in ambient mantle flow (e.g., Currie and van Wijk, 2016) where melt migration is enhanced (Holtzman and Kendall, 2010) (Fig. 7). These conditions are met at the eastern margin of the Tanzania craton where tomographic imaging indicates 50 km or more relief at the lithosphere-asthenosphere boundary (Tiberi et al., 2019). The step in lithospheric thickness is consistent with constraints from mantle xenoliths (e.g., Vauchez et al., 2005). Taken together, the spatial patterns of ϕ and δt suggest that anisotropy is enhanced by along-axis mantle flow in lithospheric thin zones augmented by oriented melt pockets and fossil anisotropy that combine to 1.5 s or more of rift-parallel anisotropy. The topographic relief at the LAB along craton margins may enhance flow, and hence melt extraction, coupling these two processes (Fig. 8).

NE-directed mantle flow from the African superplume may enhance the observed splitting, if the asthenospheric flow is faster than the slow-

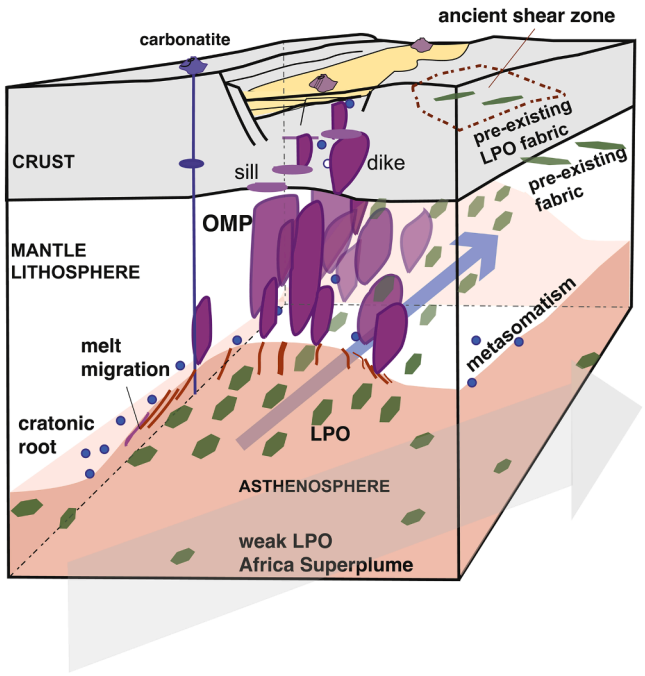

Fig. 8. Cartoon of factors contributing to the observed seismic anisotropy associated with the East African rift system (symbols not to scale). Upwelling mantle of the African Superplume (broad gray arrow) contributes a weak NE-directed anisotropy throughout the region. Zones of lithospheric thinning channel flow (blue arrow) and introduce a rift-parallel LPO fabric (green hexagons). Blue circles indicate metasomatic fluids (CO_2, H_2O). Shear zones and metamorphic fabrics within the lithosphere may locally contribute. Pressure gradients at the steep edges at the lithosphere-asthenosphere boundary guide melt (red lines) that rises into the lithosphere as blade-shaped dikes, and sub-horizontal sills; the fluid-filled cracks have small aspect ratios (e.g., Kendall et al., 2005; Hammond and Kendall, 2016).

moving plate (e.g., Fishwick and Bastow 2011) (Fig. 8). Our regional analyses support more local rift studies showing evidence for bottom-up processes driving extension in Africa, as indicated by widespread metasomatism and significantly larger amounts of mantle lithospheric thinning as opposed to mechanical crustal stretching (e.g., Wölbern et al., 2012; Hopper et al., 2020). Pre-existing lithospheric strain fabrics are not pervasive or may have been weakened in some areas by metasomatism (e.g., Snyder and Lockhart 2009). Topography at the lithosphere-asthenosphere boundary may pre-dispose craton edges to magmatism and subsequent faulting. The enhanced flow at craton edges, metasomatic alteration of the base of the plate, and progressive melt intrusion may explain the initiation of rifting in thick cratonic lithosphere.

6. Conclusions

We analyzed data from five networks (XJ, 9I/6R, 1C, YY, Sweden-Kenya) and re-analysed publicly available data from 13 African broadband networks spanning 1994 through 2022 using consistent criteria to evaluate both splitting direction (φ) and amount (δt). Rift parallel anisotropy is observed in both magma-rich and magma-poor rift sectors, but δt is largest in magmatic rift zones. The largest delay times (> 2 s) are found in the Ethiopian flood basalt province where dikes and sills span the entire lithospheric thickness. Cratonic areas outside the rifts have the smallest δt (≤ 0.5 s) with generally NE-directed φ, which may indicate an African Superplume contribution. The observed parallelism of splitting directions with sub N-S trending zones of lithospheric thinning and magmatism, indications for shallow sources of anisotropy, and spatial patterns of φ and δt indicate that anisotropy arises from strain fabrics created by along-axis mantle flow in lithospheric thin zones augmented by oriented melt pockets and fossil strain fabrics. The evidence for shallow contributions at craton edges, metasomatic alteration of the base of the plate, and progressive melt intrusion may explain the initiation of rifting in thick cratonic lithosphere. Contributions from pre-existing lithospheric strain fabrics are < 1 s, perhaps in part owing to the pervasive metasomatism above the relatively volatile-rich mantle upwelling(s).

CRediT authorship contribution statement

C.J. Ebinger: Writing – review & editing, Writing – original draft, Visualization, Validation, Project administration, Investigation, Funding acquisition, Data curation, Conceptualization. **Miriam C. Reiss:** Writing – review & editing, Visualization, Software, Methodology, Formal analysis, Data curation, Conceptualization. **Ian Bastow:** Writing – review & editing, Validation, Investigation, Funding acquisition, Data curation. **Mary M. Karanja:** Writing – review & editing, Formal analysis.

Declaration of competing interest

The authors declare that they have no known competing financial interests or personal relationships that could have appeared to influence the work reported in this paper. The authors declare the following financial interests/personal relationships which may be considered as potential competing interests.

Data availability

All data are available and data sources provided.

Acknowledgments and Data

We are grateful for the thoughtful and constructive feedback of two reviewers and editor Hans Thybo. The field deployments would not have been possible without the efforts of Steve Roecker and Christel Tiberi, the CRAFTI, CoLibREA teams, and the TRAILS teams. The work of CE, MK was supported by NSF grant EAR-1824417. CE acknowledges NSF grants EAR-1113355, 2039963, 2151594, and ANR-12-JS06-000401. IB's work was supported by the Natural Environment Research Council, grant number NE/L002515/1. For the purpose of open access, the author has applied a Creative Commons Attribution (CC BY) licence to any Author Accepted Manuscript (AAM) version arising. Seismic data are archived at the IRIS Data Management Center, and station-by-station results for the CRAFTI and 1C data sets can be found in the Supporting Information. Seismic data for the permanent GeoForschungZentrum (http://geofon.gfz-potsdam.de/) LODK and KIBK stations and KV network were sourced from ORFEUS (https://www.orfeus-eu.org).

Supplementary materials

Supplementary material associated with this article can be found, in the online version, at doi:10.1016/j.epsl.2023.118488.

References

Albaric, J., Déverchère, J., Perrot, J., Jakovlev, A., Deschamps, A., 2014. Deep crustal earthquakes in North Tanzania, East Africa: interplay between tectonic and magmatic processes in an incipient rift. Geochem. Geophys. Geosyst. 15 (2), 374–394.

Andriampenomanana, F., Nyblade, A., Durrheim, R., Tugume, F., Nyago, J., 2021. Shear wave splitting measurements in northeastern Uganda and southeastern Tanzania: corroborating evidence for sublithospheric mantle flow beneath East Africa. Geophys. J. Int. 226 (3), 1696–1704.

Argus, D.F., Gordon, R.G., DeMets, C., 2011. Geologically current motion of 56 plates relative to the no-net-rotation reference frame. Geochem. Geophys. Geosyst. 12 (11).

Baptiste, V., Tommasi, A., Vauchez, A., Demouchy, S., Rudnick, R.L., 2015. Deformation, hydration, and anisotropy of the lithospheric mantle in an active rift: constraints from mantle xenoliths from the North Tanzanian Divergence of the East African Rift. Tectonophysics 639, 34–55.

Barruol, G., Hoffman, R., 1999. Seismic anisotropy beneath the Geoscope stations from SKS splitting. J. Geophys. Res. 104 (10), 757–774.

Bastow, I.D., Pilidou, S., Kendall, J.M., Stuart, G.W., 2010. Melt-induced seismic anisotropy and magma assisted rifting in Ethiopia: evidence from surface waves. Geochem. Geophys. Geosyst. 11 (6) https://doi.org/10.1029/2010GC003036.

Becker, T.W., Chevrot, S., Schulte-Pelkum, V., Blackman, D.K., 2006. Statistical properties of seismic anisotropy predicted by upper mantle geodynamic models. J. Geophys. Res. Solid Earth 111 (B8). https://doi.org/10.1029/2005JB004095.

Bialas, R.W., Buck, W.R., Qin, R., 2010. How much magma is required to rift a continent? Earth Planet. Sci. Lett. 292 (1–2), 68–78.

Birhanu, Y., Bendick, R., Fisseha, S., Lewi, E., Floyd, M., King, R., Reilinger, R., 2016. GPS constraints on broad scale extension in the Ethiopian Highlands and Main Ethiopian Rift. Geophys Res Lett 43 (13), 6844–6851.

Bollmann, T.A., van der Lee, S., Frederiksen, A.W., Wolin, E., Revenaugh, J., Wiens, D.A., Darbyshire, F.A., Stein, S., Wysession, M.E., Jurdy, D, 2019. P wave teleseismic traveltime tomography of the North American Midcontinent. J. Geophys. Res. Solid Earth 124 (2), 1725–1742.

Boniface, N., Appel, P., 2018. Neoproterozoic reworking of the Ubendian Belt crust: implication for an orogenic cycle between the Tanzania Craton and Bangweulu Block during the assembly of Gondwana. Precambrian Res. 305, 358–385.

Boyce, A., Bastow, I., Ebinger, C.J., Cottaar, S., 2023. Insights into East African Flood Basalts, Rifting and topography revealed by new constraints on mantle wavespeed and discontinuity structure below the Turkana Depression. Geochem. Geophys. Geosyst. in press.

Casagli, A., Frezzotti, M.L., Peccerillo, A., Tiepolo, M., De Astis, G., 2017. (Garnet)-spinel peridotite xenoliths from Mega (Ethiopia): evidence for rejuvenation and dynamic thinning of the lithosphere beneath the southern Main Ethiopian Rift. Chem. Geol. 455, 231–248.

Chambers, E.L., Harmon, N., Keir, D., Rychert, C.A., 2019. Using ambient noise to image the northern East African Rift. Geochem. Geophys. Geosyst. 20 (4), 2091–2109.

Chang, S.J., Kendall, E., Davaille, A., Ferreira, A.M., 2020. The evolution of mantle plumes in East Africa. J. Geophys. Res. Solid Earth 125 (12), e2020JB019929.

Chevrot, S., 2000. Multichannel analysis of shear wave splitting. J. Geophys. Res. Solid Earth 105 (B9), 21579–21590.

Chevrot, S., 2006. Finite-frequency vectorial tomography: a new method for high-resolution imaging of upper mantle anisotropy. Geophys. J. Int. 165 (2), 641–657.

Conrad, C.P., Behn, M.D., 2010. Constraints on lithosphere net rotation and asthenospheric viscosity from global mantle flow models and seismic anisotropy. Geochem. Geophys. Geosyst. 11 (5) https://doi.org/10.1029/2009GC002970.

Craig, T.J., Jackson, J.A., Priestley, K., McKenzie, D., 2011. Earthquake distribution patterns in Africa: their relationship to variations in lithospheric and geological structure, and their rheological implications. Geophys. J. Int. 185 (1), 403–434.

Currie, C.A., van Wijk, J., 2016. How craton margins are preserved: insights from geodynamic models. J Geodyn 100, 144–158.

Daly, M.C., Green, P., Watts, A.B., Davies, O., Chibesakunda, F., Walker, R., 2020. Tectonics and landscape of the central African Plateau and their implications for a propagating Southwestern Rift in Africa. Geochem. Geophys. Geosyst. 21, e2019GC008746.

Debayle, E., Ricard, Y., 2013. Seismic observations of large-scale deformation at the bottom of fast-moving plates. Earth Planet. Sci. Lett. 376, 165–177.

Doubrovine, P.V., Steinberger, B., Torsvik, T.H., 2012. Absolute plate motions in a reference frame defined by moving hot spots in the Pacific, Atlantic, and Indian oceans. J. Geophys. Res. Solid Earth 117 (B9). https://doi.org/10.1029/2011JB009072.

Ebinger, C.J., Keir, D., I. Bastow, K. Whaler, J. Hammond, A. Ayele, M.S. Miller, C. Tiberi, S. Hautot (2017), Crustal structure of rift zones in Africa: implications for global crustal processes, in Gu, J., Ed., Special Issue of Tectonics, doi:10.1002/2017TC004526.

Ebinger, C.J., Jackson, J.A., Foster, A.N., Hayward, N.J., 1999. Extensional basin geometry and the elastic lithosphere. Philos. Trans. R. Soc. Lond. Ser. A Math. Phys. Eng. Sci. 357 (1753), 741–765.

Eilon, Z., Abers, G.A., Jin, G., Gaherty, J.B., 2014. Anisotropy beneath a highly extended continental rift. Geochem. Geophys. Geosyst. 15 (3), 545–564.

Fishwick, S., Bastow, I.D., 2011. Towards a better understanding of African topography: a review of passive-source seismic studies of the African crust and upper mantle. Geol. Soc. Lond. Spec. Public. 357 (1), 343–371.

Franke, D., Jokat, W., Ladage, S., Stollhofen, H., Klimke, J., Lutz, R., Mahanjane, E.S., Ehrhardt, A., Schreckenberger, B., 2015. The offshore East African Rift System: structural framework at the toe of a juvenile rift. Tectonics 34, 2086–2104.

Fritz, H., Abdelsalam, M., Ali, K.A., Bingen, B., Collins, A.S., Fowler, A.R., Ghebreab, W., Hauzenberger, C.A., Johnson, P.R., Kusky, T.M., Macey, P., 2013. Orogen styles in the East African Orogen: a review of the Neoproterozoic to Cambrian tectonic evolution. J. Afr. Earth Sci. 86, 65–106.

Gao, S., Davis, P.M., Liu, H., Slack, P.D., Rigor, A.W., Zorin, Y.A., Mordvinova, V.V., Kozhevnikov, V.M., Logatchev, N.A., 1997. SKS splitting beneath continental rift zones. J. Geophys. Res. 102 (B10), 22781–22797. https://doi.org/10.1029/97JB01858.

Geirsson, H., d'Oreye, N., Mashagiro, N., Syauswa, M., Celli, G., Kadufu, B., Smets, B., Kervyn, F., 2017. Volcano-tectonic deformation in the Kivu Region, Central Africa: results from six years of continuous GNSS observations of the Kivu Geodetic Network (KivuGNet). J. Afr. Earth Sci. 134, 809–823.

Global Volcanism Program, 2013. Volcanoes of the World. v 4.10.1, Venzke, E. Smithsonian Institution. https://doi.org/10.5479/si/GVP.VOTW4-2013. Downloaded 04 Jul 2021.

Hammond, J.O., Kendall, J.M., 2016. Constraints on melt distribution from seismology: a case study in Ethiopia. Spec. Public. 420, 127–147.

Holtzman, B.K., Kendall, J.M., 2010. Organized melt, seismic anisotropy, and plate boundary lubrication. Geochem. Geophys. Geosyst. 11 https://doi.org/10.1029/2010GC003296.

Homuth, B., Löbl, U., Batte, A.G., Link, K., Kasereka, C.M., Rümpker, G., 2016. Seismic anisotropy of the lithosphere/asthenosphere system beneath the Rwenzori region of the Albertine Rift. Int. J. Earth Sci. 105 (6), 1681–1692.

Hopper, E., Gaherty, J.B., Shillington, D.J., Accardo, N.J., Nyblade, A.A., Holtzman, B.K., Havlin, C., Scholz, C.A., Chindandali, P.R., Ferdinand, R.W., Mulibo, G.D., 2020. Preferential localized thinning of lithospheric mantle in the melt-poor Malawi Rift. Nat. Geosci. 13 (8), 584–589.

Kaeser, B., Kalt, A., Pettke, T., 2006. Evolution of the lithospheric mantle beneath the Marsabit volcanic field (northern Kenya): constraints from textural, P–T and geochemical studies on xenoliths. J. Petrol. 47 (11), 2149–2184.

Kaczmarek, M.A., Reddy, S.M., 2013. Mantle deformation during rifting: constraints from quantitative microstructural analysis of olivine from the East African Rift (Marsabit, Kenya). Tectonophysics 608, 1122–1137.

Kendall, J.M., Stuart, G.W., Ebinger, C.J., Bastow, I.D., Keir, D., 2005. Magma-assisted rifting in Ethiopia. Nature 433 (7022), 146–148.

Knappe, E., Bendick, R., Ebinger, C., Birhanu, Y., Lewi, E., Floyd, M., King, R., Kianji, G., Mariita, N., Temtime, T., Waktola, B., 2020. Accommodation of East African rifting across the Turkana depression. J. Geophys. Res. Solid Earth 125 (2), e2019JB018469.

Kolawole, F., Atekwana, E.A., Laó-Dávila, D.A., Abdelsalam, M.G., Chindandali, P.R., Salima, J., Kalindekafe, L., 2018. Active deformation of Malawi rift's north basin Hinge zone modulated by reactivation of preexisting Precambrian Shear zone fabric. Tectonics 37 (3), 683–704.

Kounoudis, R., Bastow, I.D., Ebinger, C.J., Ogden, C.S., Ayele, A., Bendick, R., Mariita, N., Kianji, G., Wigham, G., Musila, M., Kibret, B., 2021. Body-Wave Tomographic Imaging of the Turkana Depression: implications for Rift Development and Plume-Lithosphere Interactions. Geochem. Geophys. Geosyst. 22 (8), e2021GC009782.

Lavayssière, A., C. Drooff, C.J. Ebinger, R. Gallacher, F. Illsley-Kemp, S. Oliva, D.B. Keir, K. Mtelela, (2019). Along-axis segmentation and lower crustal earthquakes: Seismicity of the southern Tanganyika rift zone, Tectonics, doi:10.1029/2018TC005379.

Liu, J., Pearson, D.G., Wang, L.H., Mather, K.A., Kjarsgaard, B.A., Schaeffer, A.J., Irvine, G.J., Kopylova, M.G., Armstrong, J.P., 2021. Plume-driven recratonization of deep continental lithospheric mantle. Nature 592, 732–736.

Lopes, E., Long, M.D., Karabinos, P., Aragon, J.C., 2020. SKS splitting and upper mantle anisotropy beneath the southern New England Appalachians: constraints from the dense SEISConn array. In: Geochem. Geophys. Geosyst., 21, e2020GC009401.

Mainprice, D., 1997. Modelling the anisotropic seismic properties of partially molten rocks found at mid-ocean ridges. Tectonophysics 279, 161–179.

Muirhead, J., Fischer, T.P., Oliva, S.J., Laizer, A., Judd, E.J., Lee, H., Kazimoto, E., Sano, Y., Takahata, N., Tiberi, C., van Wijk, J., Dufek, J., Foley, S., Currie, C., Ebinger, C.J., 2020. Displacement of cratonic mantle and lithospheric channeling concentrates deep carbon during continental rifting. Nature 582.

Muirhead, J.D., Kattenhorn, S.A., 2018. Activation of preexisting transverse structures in an evolving magmatic rift in East Africa. J. Struct. Geol. 106, 1–18.

Musila, M., C.J. Ebinger, I.D. Bastow, G. Sullivan, S.J. Oliva, E. Knappe, M. Perry, R. Kounoudis, C.S. Ogden, R. Bendick, S. Mwangi, N. Mariita, G. Kianji, E. Klein, F. Illsley-Kemp, Strain accommodation during continental rifting: mantle lithosphere matters, Geochem. Geophys. Geosyst., e2023GC010982 2023.

Nicolas, A., & Christensen, N.I. (1987). Formation of anisotropy in upper mantle peridotites-a review. Composition, Structure and Dynamics of the Lithosphere-Asthenosphere System, 16, 111–123.

Ogden, C.S., Bastow, I.D., Ebinger, C., Ayele, A., Kounoudis, R., Musila, M., Bendick, R., Mariita, N., Kianji, G., Rooney, T.O., Sullivan, G., 2023. The development of multiple phases of superposed rifting in the Turkana Depression, East Africa: evidence from receiver functions. Earth Planet. Sci. Lett. 609, 118088.

Pik, B.Marty, Hilton, D.R., 2006. How many mantle plumes in Africa? The geochemical point of view. Chem. Geol.. https://doi.org/10.1016/j.chemgeo.2005.09.016.

Rajaonarison, T., D.S. Stamps, J. Naliboff, A. Nyblade, E. Njinju (2023), Geodynamic investigation of plume-lithosphere interactions beneath the East African Rift, doi:10.1029/2022JB025800.

Reiss, M.C., Rümpker, G., 2017. SplitRacer: MATLAB code and GUI for semiautomated analysis and interpretation of teleseismic shearwave splitting. Seismol. Res. Lett. 88, 392. https://doi.org/10.1785/0220160191.

Reiss, M.C., Long, M.D., Creasy, N., 2019. Lowermost mantle anisotropy beneath Africa from differential SKS-SKKS shear-wave splitting. J. Geophys. Res. Solid Earth 124.

Ritsema, J., Deuss, A., Van Heijst, H.J., Woodhouse, J.H., 2011. S40RTS: a degree-40 shear-velocity model for the mantle from new Rayleigh wave dispersion, teleseismic traveltime and normal-mode splitting function measurements. Geophys. J. Int. 184 (3), 1223–1236.

Roberts, E.M., Stevens, N.J., O'Connor, P.M., Dirks, P.H.G.M., Gottfried, M.D., Clyde, W. C., Armstrong, R.A., Kemp, A.I.S., Hemming, S., 2012. Initiation of the western branch of the East African Rift coeval with the eastern branch. Nat. Geo 5 (4), 289–294. https://doi.org/10.1038/ngeo1432.

Rudnick, R.L., Ireland, T.R., Gehrels, G., Irving, A.J., Chesley, J.T., & Hanchar, J.M. (1998, April). Dating mantle metasomatism: u-Pb geochronology of zircons in

cratonic mantle xenoliths from Montana and Tanzania. In International Kimberlite Conference: Extended Abstracts (Vol. 7, pp. 754–756).
Rümpker, G., Ryberg, T., 2000. New 'Fresnel-zone' estimates for shear-wave splitting observations from finite-difference modeling. Geophys. Res. Lett. 27, 2005–2008.
Saria, E., Calais, E., Stamps, D.S., Delvaux, D., Hartnady, C.J.H., 2014. Present-day kinematics of the East African Rift. J. Geophys. Res. Solid Earth 119 (4), 3584–3600.
Silver, P.G., Chan, W.W., 1991. Shear wave splitting and subcontinental mantle deformation. J. Geophys. Res. 96 (B10), 16429–16454. https://doi.org/10.1029/91JB00899.
Silver, P.G., Long, M.D., 2011. The non-commutivity of shear wave splitting operators at low frequencies and implications for anisotropy tomography. Geophys. J. Int. 184, 1415–1427.
Sleep, N.H., Ebinger, C.J., Kendall, J.M., 2002. Deflection of Mantle Plume Material by Cratonic Keels. Special Publications, London, pp. 135–150. Geological Society199.
Snyder, D.B., Lockhart, G., 2009. Does seismically anisotropic subcontinental mantle lithosphere require metasomatic wehrlite–pyroxenite dyke stockworks? Lithos 112, 961–965.
Stamps, D.S., Flesch, L.M., Calais, E., 2010. Lithospheric buoyancy forces in Africa from a thin sheet approach. Int. J. Earth Sci. 99, 1525–1533.
Stamps, D.S., Saria, E., Kreemer, C., 2018. A geodetic strain rate model for the East African Rift System. Sci. Rep. 8 (1), 732.
Tepp, G., Ebinger, C.J., Zal, H., Gallacher, R., Accardo, N., Shillington, D.J., et al., 2018. Seismic anisotropy of the upper mantle below the western rift, East Africa. J. Geophys. Res. Solid Earth. https://doi.org/10.1029/2017jb015409.
Tiberi, C., Gautier, S., Ebinger, C., Roecker, S., Plasman, M., Albaric, J., Déverchère, J., Peyrat, S., Perrot, J., Wambura, R.F., Msabi, M., 2019. Lithospheric modification by extension and magmatism at the craton-orogenic boundary: north Tanzania Divergence, East Africa. Geophys. J. Int. 216, 1693–1710.
Tommasi, A., Baptiste, V., Vauchez, A., Holtzman, B., 2016. Deformation, annealing, reactive melt percolation, and seismic anisotropy in the lithospheric mantle beneath the southeastern Ethiopian rift: constraints from mantle xenoliths from Mega. Tectonophysics 682, 186–205.
Tommasi, A., Vauchez, A., 2015. Heterogeneity and anisotropy in the lithospheric mantle. Tectonophysics 661, 11–37.
Trestrail, K.R., Rooney, T.O., Girard, G., Svoboda, C., Yirgu, G., Ayalew, D., Keppelman, J., 2017. Sub-continental lithospheric mantle deformation in the Yerer-Tullu Wellel Volcanotectonic Lineament: a study of peridotite xenoliths. Chem. Geol. 455, 249–263.
Vauchez, A., Dineur, F., Rudnick, R., 2005. Microstructure, texture and seismic anisotropy of the lithospheric mantle above a mantle plume: insights from the Labait volcano xenoliths (Tanzania). Earth Planet. Sci. Lett. 232, 295–314.
Walker, K.T., Nyblade, A.A., Klemperer, S.L., Bokelmann, G.H.R., Owens, T.J., 2004. On the relationship between extension and anisotropy: constraints from shear wave splitting across the East African Plateau. J. Geophys. Res. 109, B08302. https://doi.org/10.1029/2003JB002866.
Wölbern, I., Rümpker, G., Link, K., Sodoudi, F., 2012. Melt infiltration of the lower lithosphere beneath the Tanzania craton and the Albertine rift inferred from S receiver functions. Geochem. Geophys. Geosyst. 13 (8).